

Banner appropriate to article type will appear here in typeset article

# Transient Growth in Streaky Unbounded Shear Flow: A symbiosis of Orr and Push-over mechanisms

William Oxley<sup>1</sup> and Rich R. Kerswell<sup>1</sup>

<sup>1</sup>DAMTP, Centre for Mathematical Sciences, Wilberforce Road, Cambridge CB3 0WA, UK

(Received xx; revised xx; accepted xx)

Transient growth mechanisms operating on streaky shear flows are believed important for sustaining near-wall turbulence. Of the three individual mechanisms present - Orr, lift-up and ‘push-over’ - Lozano-Duran *et al.* (*J. Fluid Mech.* **914**, A8, 2021) have recently observed that both Orr and push-over need to be present to sustain turbulent fluctuations given streaky (streamwise-independent) base fields whereas lift-up does not. We show here, using Kelvin’s model of unbounded constant shear augmented by spanwise streaks, that this is because the push-over mechanism can act in concert with a ‘spanwise’ Orr mechanism to produce much-enhanced transient growth. In a reduced representation of the process which captures the growth properties of the full system, the optimal disturbance growth scales like  $G \sim e^{\alpha\sqrt{Re}}$  ( $\alpha$  a constant and  $Re$  the Reynolds number) for near-wall streak shears over ‘intermediate’  $O(\sqrt{Re})$  times, in contrast with the usual algebraic result of  $G \sim Re^2$  produced by Orr or push-over separately over ‘slow’  $O(Re)$  times. Our results therefore support the view that while lift-up is believed central for the roll-to-streak regenerative process, it is Orr and push-over mechanisms that are *both* key for the streak-to-roll regenerative process in near-wall turbulence.

## 1. Introduction

Efforts to understand wall-bounded turbulence have naturally focussed on the wall and the (coherent) structures which form there (Richardson 1922). The consensus is that there is (at least) a near-wall sustaining cycle (Hamilton *et al.* 1995; Waleffe 1997; Jimenez & Pinelli 1999) involving predominantly streaks and streamwise rolls (or vortices) which helps maintain the turbulence (e.g. see the reviews Robinson 1991; Panton 2001; Smits *et al.* 2011; Jimenez 2012, 2018). The generation of these streaks from the rolls is commonly explained by the (linear) transient growth ‘lift-up’ mechanism (Ellingsen & Palm 1975; Landahl 1980), but how rolls are regenerated from the streaks has proven a little less clear due to the need to invoke nonlinearity at some point.

Just focusing on the initial linear part, Schoppa & Hussain (2002) suggested that transient growth mechanisms on the streaks were actually more important than (linear) streak instabilities, and that it was these transiently growing perturbations which fed back to create streaks through their nonlinear interaction. While this view has been contested (e.g. Hoepffner *et al.* 1995; Cassinelli *et al.* 2017; Jimenez 2018), it is supported by recent cause-and-effect numerical experiments by Lozano-Durán *et al.* (2021) who looked more closely

**Abstract must not spill onto p.2**

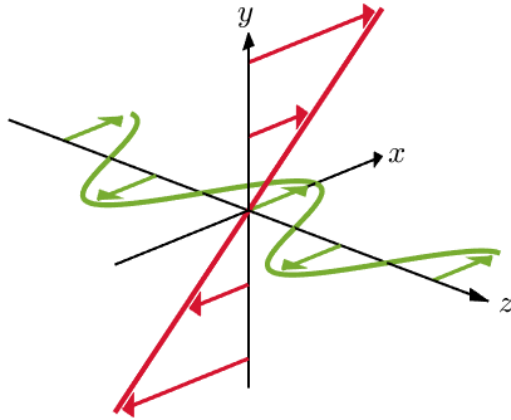


**Figure 1:** The streaky unbounded shear flow studied here: see equation (2.1). The (green) spanwise streaks extend Kelvin’s (red) popular constant shear model.

at all the linear processes present. In particular, Lozano-Durán *et al.* (2021) isolated the influence of the three different transient growth mechanisms: the familiar Orr (Orr 1907) and lift-up (Ellingsen & Palm 1975) mechanisms present for a 1D shear profile  $U(y)$  and a far less-studied ‘push-over’ mechanism which can only operate when the base profile has spanwise shear i.e.  $U(y, z)$ . They found, somewhat unexpectedly, that the Orr and push-over mechanisms are *both* essential to maintain near-wall turbulence when streaky base flows were prescribed but lift-up is not: see their §6.4 and figure 24(a).

Markeviciute & Kerswell (2024) investigated this further by looking at the transient growth possible on a wall-normal shear plus monochromatic streak field consistent with the buffer region at the wall. Over appropriately short times (e.g. one eddy turnover time as proposed by Butler & Farrell (1993)), they found a similarly clear signal that lift-up is unimportant whereas the removal of push-over dramatically reduced the growth: see their figure 7. The necessity to have push-over operating with the Orr mechanism indicates they are working symbiotically. How this happens, however, is puzzling from the timescale perspective as Orr is considered a ‘fast’ mechanism which operates over inertial timescales whereas push-over looks a ‘slow’ mechanism operating over viscous timescales. This latter characterisation comes from an analogy with lift-up in which viscously-decaying wall-normal velocities (as present in streamwise rolls) advect the base shear to produce streaks. Push-over (a term coined by Lozano-Durán *et al.* (2021)) similarly involves viscously-decaying spanwise velocities advecting the spanwise streak shear. Understanding exactly how these two mechanisms constructively interact is therefore an interesting issue.

The purpose of this paper is to lay bare this interaction by exploring it in an augmented version of Kelvin’s famous constant shear model (Kelvin 1887). This simple model - an unbounded shear  $\mathbf{U} = y\hat{\mathbf{x}}$  (just the red flow in figure 1) - was used by Orr (1907) for his seminal work and has been important in clarifying the characteristics of both Orr and lift-up mechanisms subsequently (e.g. Farrell & Ioannou 1993; Jimenez 2013; Jiao *et al.* 2021) and as a shear-flow testbed otherwise (e.g. Moffatt 1967; Marcus & Press 1977). The key features of the model are that the base flow is: 1. unbounded and so not restricted by any boundary conditions; and 2. a linear function of space. These together permit plane wave solutions to the perturbation evolution equations where the spatially-varying base advection can be accounted for by time-dependent wavenumbers. This leaves just 2 ordinary differential equations (ODEs) for the cross-shear velocity and cross-shear vorticity to be integrated forward in time. These ‘Kelvin’ modes form a complete set but, unusually, are

not individually separable in space and time and so the representation differs from the usual plane wave approach with constant wavenumbers. Kelvin and Orr used these modes to study unidirectional shear but they can also be used more generally to study the stability of time-dependent spatially-linear flows (Craik & Criminale 1986; Craik 1989), flows with closed streamlines such as elliptical (Bayly 1986; Landman & Saffman 1987; Waleffe 1990) and precessing flows (Kerswell 1993), or flows with more physics included such as stratification (Hartman 1975; Miyazaki & Fukumoto 1992), rotation (Tung 1983; Salhi & Cambon 2010) or magnetic fields (Craik 1988).

The augmented base flow considered here - shown in Figure 1 and equation (2.1) below - builds in a streak field which introduces spatially-periodic spanwise shear. This is now not purely linear in space and so a Kelvin mode is no longer a solution of the linearised perturbation equations. Instead, a single sum of Kelvin modes over spanwise wavenumbers is needed, but, importantly, the wall-normal shear can be handled as usual, removing the unbounded advective term from the system. This means the model system is still a very accessible ‘sandbox’ in which to study the transient growth mechanisms of Orr, lift-up and now, crucially, also ‘push-over’. The price to be paid for introducing the streak field is an order of magnitude increase in the number of ODEs to be solved, but, since this is increased from 2 to  $O(20)$ , it is trivial by today’s standards.

The plan of the paper is as follows. Section 2 introduces the model, the evolution equations and discusses appropriate parameter values. Section 3 revisits Kelvin’s unbounded constant-shear model, presenting some new large- $Re$  asymptotic scaling laws and discussing the timescales for Orr and lift-up growth mechanisms. The presence of streaks is introduced in §4, with the 2D limit of no streamwise variation used in §4.1 to illustrate how the push-over mechanism behaves when it acts alone. This is followed by a general analysis of the transient growth possible for the full 3D system in §4.2 which is found to clearly capture the symbiotic relationship between Orr and push-over. Section 4.3 then describes a severely truncated system which lays bare how Orr and push-over help each other to generate enhanced growth. This system allows some scaling predictions to be made which are then shown to hold true in the full 3D system. A final discussion follows in §5.

## 2. Formulation

### 2.1. Governing Equations

We consider a unidirectional base flow velocity in the  $x$ -direction which has a constant shear in  $y$  and a spatially periodic ‘streak’ shear varying in the spanwise  $z$ -direction,

$$\mathbf{U}_B = U_B(y, z)\mathbf{e}_x = [y + \beta \cos(k_z z)]\mathbf{e}_x, \quad (2.1)$$

where  $\beta$  is the dimensionless streak strength: see Figure 1. The system has been non-dimensionalised by the  $y$ -shear rate,  $S$ , and the initial  $k_y$  wavenumber (i.e. by a lengthscale  $L := L_y/2\pi$  where  $L_y$  is the initial perturbation wavelength in  $y$ ), so that the streak wavenumber  $k_z$  is a parameter of the problem. This allows straightforward access to the well-studied Kelvin problem of  $\beta \rightarrow 0$  while using the spanwise wavenumber as an inverse length scale does not.

The Navier-Stokes equations linearised around  $\mathbf{U}_B$  for a perturbation  $\mathbf{u} := (u, v, w)$  and associated pressure perturbation  $p$  are then

$$\frac{\partial \mathbf{u}}{\partial t} + [y + \beta \cos(k_z z)] \frac{\partial \mathbf{u}}{\partial x} + [v - \beta w k_z \sin(k_z z)]\mathbf{e}_x + \nabla p = \frac{1}{Re} \Delta \mathbf{u}, \quad (2.2)$$

$$\nabla \cdot \mathbf{u} = 0. \quad (2.3)$$

Here, the Reynolds number is  $Re := L^2 S / \nu$ , where  $\nu$  is the kinematic viscosity. Taking  $\mathbf{e}_y \cdot \nabla \times$  and  $\mathbf{e}_y \cdot \nabla \times \nabla \times$  of (2.2) leads to a pair of equations for  $v$ , and the  $y$ -shearwise vorticity,  $\eta := \partial u / \partial z - \partial w / \partial x$ ,

$$\left[ \frac{\partial}{\partial t} + [y + \beta \cos(k_z z)] \frac{\partial}{\partial x} - \frac{1}{Re} \Delta \right] \Delta v + 2\beta k_z \sin(k_z z) \left[ \frac{\partial^2 w}{\partial x \partial y} - \frac{\partial^2 v}{\partial x \partial z} \right] - \beta k_z^2 \cos(k_z z) \frac{\partial v}{\partial x} = 0, \quad (2.4)$$

$$\left[ \frac{\partial}{\partial t} + [y + \beta \cos(k_z z)] \frac{\partial}{\partial x} - \frac{1}{Re} \Delta \right] \eta + \frac{\partial v}{\partial z} + \beta k_z \sin(k_z z) \frac{\partial v}{\partial y} - \beta w k_z^2 \cos(k_z z) = 0. \quad (2.5)$$

## 2.2. Kelvin Modes

The well-known trick to handle the  $y$ -dependent advection term is to allow the wavenumbers of the perturbation to be time-dependent (Kelvin 1887) giving a ‘Kelvin’ mode

$$[u, v, w, p, \eta](x, y, z, t) = [\hat{u}, \hat{v}, \hat{w}, \hat{p}, \hat{\eta}](t) e^{i[k_x x + (1 - k_x t)y + k_z z]}, \quad (2.6)$$

which is actually a full solution to the unlinearised perturbation equations since  $\mathbf{k} \cdot \mathbf{u} = 0$  by incompressibility (e.g. Craik & Criminale 1986). For  $\beta \neq 0$ , the extra streak shear unavoidably couples different spanwise wavenumbers and the perturbation ansatz has to be extended to

$$[u, v, w, p, \eta](x, y, z, t) = \sum_{m=-M}^M [\hat{u}_m, \hat{v}_m, \hat{w}_m, \hat{p}_m, \hat{\eta}_m](t) e^{i[k_x x + (1 - k_x t)y + m k_z z]}, \quad (2.7)$$

where, formally,  $M$  should be infinite but, practically, is chosen large enough so as not to influence the results. This ansatz could be extended further by shifting the spanwise wavenumbers by a fraction of the base wavenumber - so  $m k_z \rightarrow m k_z + \mu$  where  $-\frac{1}{2} k_z \leq \mu < \frac{1}{2} k_z$  (the modulation parameter in Floquet theory) - but only  $\mu = 0$  is treated here consistent with numerical observations e.g. Schoppa & Hussain (2002). Also, since  $\mathbf{U}_B$  is symmetric about  $z = 0$ , perturbations which are either symmetric (‘varicose’) or antisymmetric (‘sinuous’) in  $u$  about  $z = 0$  can be pursued separately. However, the computations are sufficiently low-cost that it was easier to just consider both cases together.

The continuity equation and definition of  $\eta$  make it possible to express  $\hat{u}_m$  and  $\hat{w}_m$  in terms of  $\hat{v}_m$  and  $\hat{\eta}_m$  as follows

$$\hat{u}_m = \frac{-k_x(1 - k_x t)\hat{v}_m - i m k_z \hat{\eta}_m}{k_x^2 + m^2 k_z^2} \quad \text{and} \quad \hat{w}_m = \frac{-m k_z(1 - k_x t)\hat{v}_m + i k_x \hat{\eta}_m}{k_x^2 + m^2 k_z^2}, \quad (2.8)$$

and then equations (2.4) and (2.5) require for each integer  $m$ :

$$\begin{aligned} \dot{\hat{v}}_m + \left[ -\frac{2k_x(1 - k_x t)}{k_m^2} + \frac{k_m^2}{Re} \right] \hat{v}_m &= \frac{i\beta k_x}{2k_m^2} \left[ 2(m+1) \frac{k_z^2 k_{m+1}^2}{h_{m+1}^2} - k_z^2 - k_{m+1}^2 \right] \hat{v}_{m+1} \\ &\quad - \frac{i\beta k_x}{2k_m^2} \left[ 2(m-1) \frac{k_z^2 k_{m-1}^2}{h_{m-1}^2} + k_z^2 + k_{m-1}^2 \right] \hat{v}_{m-1} \\ &\quad + \frac{\beta k_x^2 k_z(1 - k_x t)}{k_m^2 h_{m+1}^2} \hat{\eta}_{m+1} - \frac{\beta k_x^2 k_z(1 - k_x t)}{k_m^2 h_{m-1}^2} \hat{\eta}_{m-1} \end{aligned} \quad (2.9)$$

and

$$\begin{aligned} \hat{\eta}_m + \frac{k_m^2}{Re} \hat{\eta}_m = & -\frac{ik_x \beta}{2} \left(1 - \frac{k_z^2}{h_{m+1}^2}\right) \hat{\eta}_{m+1} - \frac{ik_x \beta}{2} \left(1 - \frac{k_z^2}{h_{m-1}^2}\right) \hat{\eta}_{m-1} \\ & - imk_z \hat{v}_m - \frac{\beta k_z (1 - k_x t)}{2} \left(\frac{(m+1)k_z^2}{h_{m+1}^2} - 1\right) \hat{v}_{m+1} \\ & - \frac{\beta k_z (1 - k_x t)}{2} \left(\frac{(m-1)k_z^2}{h_{m-1}^2} + 1\right) \hat{v}_{m-1}, \end{aligned} \quad (2.10)$$

where  $h_m^2 := k_x^2 + m^2 k_z^2$  and  $k_m^2 := k_x^2 + (1 - k_x t)^2 + m^2 k_z^2$ . These  $2(2M+1)$  coupled complex ODEs are readily integrated forward in time from given initial conditions using MATLAB's ode45.

### 2.3. Kinetic Energy and Optimal Gain

The volume-averaged kinetic energy is defined as

$$E(t) := \frac{1}{V_\Omega} \int_\Omega \frac{1}{2} |\mathbf{u}(\mathbf{x}, t)|^2 d\Omega = \frac{1}{2} \sum_{m=-M}^M \frac{1}{h_m^2} \left[ k_m^2 |\hat{v}_m|^2 + |\hat{\eta}_m|^2 \right], \quad (2.11)$$

where  $\Omega := [0, 2\pi/k_x] \times [0, 2\pi] \times [0, 2\pi/k_z]$  and  $V_\Omega$  is the volume of  $\Omega$ . In this paper we define the ‘optimal gain’ as the largest value of  $E(T)/E(0)$  over all possible initial conditions,

$$G(T, k_x, k_z; \beta, Re) := \max_{\mathbf{u}(0)} \frac{E(T, k_x, k_z; \beta, Re)}{E(0, k_x, k_z; \beta, Re)}. \quad (2.12)$$

The ‘global optimal gain’ will be the result of optimising this quantity over the wavenumbers,

$$\mathcal{G}(T; \beta, Re) := \max_{\{k_x, k_z\}} G(T, k_x, k_z; \beta, Re), \quad (2.13)$$

and the ‘overall optimal gain’ will be the result of optimising this over the time  $T$ ,

$$\mathbb{G}(\beta, Re) := \max_T \mathcal{G}(T; \beta, Re). \quad (2.14)$$

### 2.4. Parameter Choices: log layer scalings

The focus in this study is to consider values for the five physical parameters -  $T, k_x, k_z, \beta$  and  $Re$  - appropriate for the buffer and lower log layer (e.g. Jimenez 2018; Lozano-Durán *et al.* 2021). At a lengthscale of  $\approx 20v/u_\tau$  from the wall - or  $y^+ = 20$  in so-called viscous wall units where  $u_\tau$  is the friction velocity at the wall, the mean velocity can be estimated from the empirical log-layer result

$$U^+(y^+) = U/u_\tau \approx \frac{1}{\kappa} \ln y^+ + B, \quad (2.15)$$

where  $\kappa \approx 0.4$  and  $B \approx 5$ . This gives a local Reynolds number of

$$Re_{\text{local}} \approx y^+ \left( \frac{1}{\kappa} \ln y^+ + B \right) \approx 250. \quad (2.16)$$

A representative  $T$  can be found using the time quoted by Lozano-Durán *et al.* (2021) for the maximum gain seen in numerical computations, which is  $t = 0.35h/u_\tau$  ( $h$  being the half-channel width) at  $Re_\tau = 180$  and comparable with the eddy turnover time at the appropriate distance from the wall (Markeviciute & Kerswell 2024). The local shear rate at  $y^+$  in the log

layer is  $S = dU/dy = Re_\tau u_\tau / h dU^+ / dy^+ = Re_\tau u_\tau / (h\kappa y^+)$  which gives a time in our inverse shear rate units of

$$T \sim 0.35 \frac{h}{u_\tau} S = 0.35 \frac{Re_\tau}{\kappa y^+} \approx 8 \quad (2.17)$$

for  $y^+ = 20$ .

A reasonable assumption is to take the initial  $k_y$  (cross-shear) wavenumber used to nondimensionalise the model as  $2\pi/y^+$  (i.e. the wavelength is the distance to the wall), so the other non-dimensionalised wavenumbers are  $k_z \sim O(y^+ / (\lambda_z^+ \approx 100))$  and  $k_x \sim O(y^+ / (\lambda_x^+ \approx 300))$ . Therefore both wavenumbers are  $O(0.1-1)$ .

The magnitude of  $\beta$  can be estimated in two ways: comparing velocities or, perhaps more relevantly, comparing shears. In terms of velocities, typical root-mean-square velocities near the wall are  $u_{rms} \approx 1$  (in units of  $u_\tau$ ). Magnifying these values by a factor of  $\sqrt{2}$  to correct for the cosine dependence assumed in (2.1) and normalising by the base flow  $U^+(20) \approx 12$  gives  $\beta \approx 0.1$ . It makes more sense, however, to compare shear rates, then

$$\frac{k_z \beta / \sqrt{2}}{1} \approx \frac{k_z u_{rms}}{1 / (\kappa y^+)} \quad (2.18)$$

which instead gives  $\beta \approx 11$  at  $y^+ = 20$ . Given this, we consider values of  $\beta$  from 1 to 5 in the below (going to higher  $\beta$  causes problems with numerical overflow in our model: see figure 8).

### 3. Unbounded Constant Shear Flow ( $\beta = 0$ ): Kelvin's problem

Removing the streaks ( $\beta = 0$ ) recovers Kelvin's classical unbounded constant shear model (Kelvin 1887) which ever since has proved a popular testing ground for ideas (e.g. Orr 1907; Moffatt 1967; Craik & Criminale 1986; Farrell & Ioannou 1993; Jimenez 2013; Jiao *et al.* 2021). The evolution equations are simply

$$(k^2 \hat{v})_t = -\frac{k^2}{Re} (k^2 \hat{v}), \quad \hat{\eta}_t = -\frac{k^2}{Re} \hat{\eta} - ik_z \hat{v}, \quad (3.1)$$

with the solution

$$\hat{v}(t) = \frac{k^2(0)}{k^2(t)} \hat{v}(0) e^{\phi(t)}, \quad \hat{\eta}(t) = \left\{ \frac{-ik_z k^2(0) \hat{v}(0)}{k_x h} [\theta(t) - \theta(0)] + \hat{\eta}(0) \right\} e^{\phi(t)}, \quad (3.2)$$

where

$$\phi(t) := -\frac{1}{Re} \int_0^t k^2(\tau) d\tau, \quad \text{and} \quad \theta(t) := \tan^{-1} \left[ \frac{h}{1 - k_x t} \right] \quad (3.3)$$

(Farrell & Ioannou 1993; Jiao *et al.* 2021). It is well known that two growth mechanisms are present which are revealed by taking the appropriate 2-dimensional special case:  $k_z = 0$  possesses the Orr mechanism (Orr 1907) only and  $k_x = 0$  possesses the lift-up mechanism (Ellingsen & Palm 1975) only.

#### 3.1. Orr mechanism

With  $k_z = 0$ , the shearwise vorticity can only exponentially decay leaving the shrinking of  $k^2(t) := k_x^2 + (1 - k_x t)^2$  with time in the expression for  $\hat{v}(t)$  - see (3.2) - the sole growth mechanism. Growth occurs for  $t \leq 1/k_x$  with the viscous (exponential) damping term moderating this. The fact that the growth time does not scale with viscosity means the Orr mechanism is inertial and so considered 'fast'.

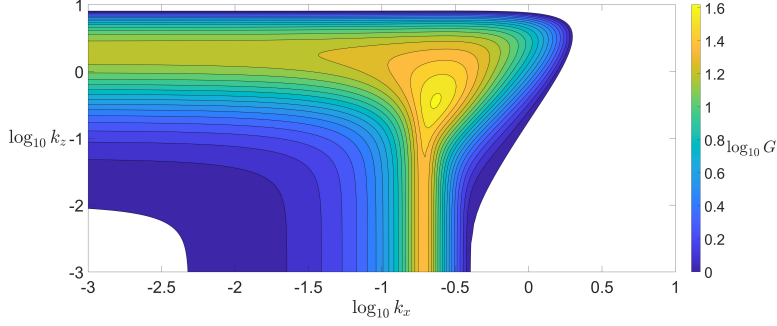


**Figure 2:** A contour plot of optimal growth  $G$  in wavenumber space for  $T = 5$  and  $Re = 200$ . This figure shows that the optimal early time gain occurs for a three-dimensional perturbation, at a location in wavenumber space close to the  $k_x$  value associated with the maximum gain possible through the Orr mechanism.

For large  $Re$  and  $1 \lesssim T = o(Re)$ , the viscous damping can be ignored and then  $k_x = \frac{1}{2}(\sqrt{T^2 + 4} - T)$  maximises the global optimal growth at

$$\mathcal{G}^{\text{Orr}} = 1/k_x^2 \sim T^2 \quad (3.4)$$

for  $T^2 \gg 4$ . For  $1 \ll T = O(Re)$ , the optimal wavenumber is still related to the time via  $k_x = 1/T$  to leading order and it is simple to show that the overall growth maximum over  $T$  (the overall global optimal) is

$$\mathbb{G}^{\text{Orr}} = \frac{9}{e^2} Re^2, \quad T^{\text{Orr}} = 3Re, \quad k_x^{\text{Orr}} = \frac{1}{3Re}, \quad (3.5)$$

where  $e = \exp(1) = 2.7183$ . So, somewhat paradoxically, the maximum growth over all times produced by the ‘fast’ Orr mechanism actually occurs on a ‘slow’ viscous time scale.

### 3.2. Lift-Up mechanism

With  $k_x = 0$ , there is no growth possible in  $\hat{v}$  but this velocity component forces the shearwise vorticity  $\hat{\eta}$  which grows. This growth ultimately is turned off by the viscous decay of  $\hat{v}$  and so lift-up is viewed as a ‘slow’ viscous process. The overall optimal lift-up growth ( $k_x = 0$ ) is,

$$\mathbb{G}^{\text{lift-up}} = \frac{4}{27e^2} Re^2, \quad T^{\text{lift-up}} = \frac{2}{3} Re, \quad k_z^{\text{lift-up}} = \frac{1}{\sqrt{2}}, \quad (3.6)$$

which is consistent with this. Here, since  $1 \ll T = O(Re)$ , the initial shearwise vorticity can be ignored facilitating the derivation of (3.6) while for  $1 \lesssim T = o(Re)$ , this is no longer valid.

### 3.3. Fully 3D optimals

Figure 2 shows the growth landscape over  $(k_x, k_z)$  plane for  $T = 5$  and  $Re = 200$ . The optimal  $k_x$  wavenumber is close to the (2D) Orr optimal value ( $k_z \rightarrow 0$  on the plot) but the optimal  $k_z$  is an order of magnitude smaller than the corresponding lift-up value ( $k_x \rightarrow 0$ ). This observation is robust over different  $T$  as shown in Figure 3(b) and becomes more exaggerated as  $T$  increases towards the maximum at  $T = O(Re)$ . It is also noticeable in 3(a) that this overall optimal gain  $\mathbb{G}$  (maximised over all  $k_x, k_z$  and  $T$ ) occurs at about the same time as the Orr maximum (this is clearly not true for lift-up). This and the  $k_x$  observation suggests using the large  $Re$  results in (3.5) for Orr as a starting point for analysing the full 3D optimal.

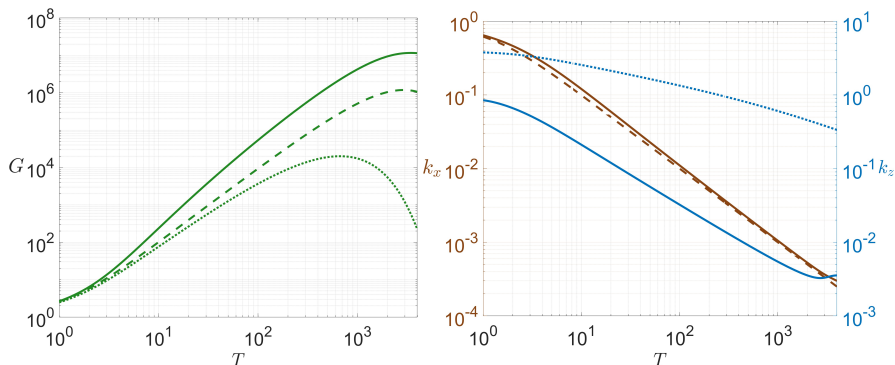


**Figure 3:** Left: optimal growth vs  $T$  at  $Re = 1000$ . The solid line is the full 3D optimal  $\mathcal{G}(Re) = \max_{(k_x, k_z)} G(k_x, k_z; Re)$ , the dashed line is  $\max_{k_x} G(k_x, 0; Re)$  (Orr) and the dotted line is  $\max_{k_z} G(0, k_z; Re)$  (lift-up). Right: the corresponding optimal wavenumbers: solid brown/blue for  $k_x/k_z$  in lift up, dashed brown for  $k_x$  in Orr and dotted blue for  $k_z$  in lift up. These plots show that the 3D optimal closely follows the Orr result in terms of both  $G$  and  $k_x$  with assistance from lift-up except near the maximum over  $T$  (the overall optimal gain  $\mathbb{G}$ ).

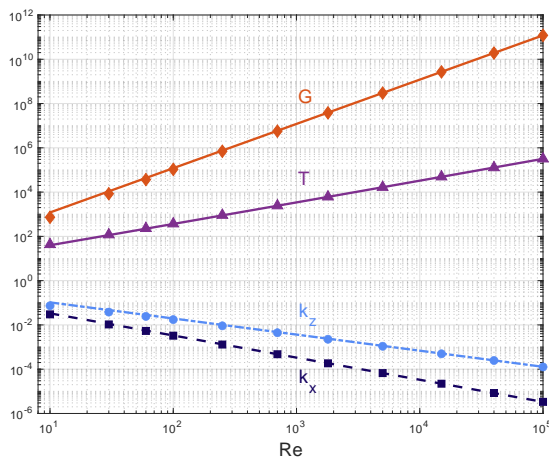


**Figure 4:** This plot shows the overall optimal gain  $\mathbb{G}(\beta, Re)$  and associated optimising parameters ( $k_x$ ,  $k_y$  and  $T$ ) as a function of  $Re$  for  $\beta = 0$  in symbols. The asymptotic predictions of (3.7) are the lines.

Assuming that the initial shearwise vorticity is zero, this leads to

$$\mathbb{G}^{3D} = \frac{9\pi^2}{e^2} Re^2, \quad T^{3D} = 3Re + \alpha Re^{9/11}, \quad k_x^{3D} = \frac{1}{3Re}, \quad k_z^{3D} = \gamma Re^{-8/11}, \quad (3.7)$$

where  $\alpha := 3^{6/11}/\pi^{2/11} \approx 1.4786$  and  $\gamma := \pi^{3/11}/3^{9/11} \approx 0.5562$ . These asymptotic predictions match our numerical computations very well even down to  $Re = O(30)$  - see Figure 4, also providing *a posteriori* justification for assuming the optimal has  $\hat{\eta}(0) = 0$ . The formulae in (3.7) give optimal wavenumbers at  $Re = 100$  of  $(k_x, k_z) = (3.33, 19.53) \times 10^{-3}$  which are consistent with figure 1(a) of Jiao *et al.* (2021).

#### 4. Early Time Transient Growth in Streaky Flow ( $\beta \neq 0$ )

We now shift our focus to streaky unbounded constant shear flow and the transient growth possible over  $O(1)$  times as discussed in §2.4. The required optimals will prove to be fully 3-dimensional but we start by looking at the reduced 2-dimensional (streamwise-independent  $k_x = 0$ ) problem which isolates the unfamiliar ‘push-over’ mechanism.

##### 4.1. 2-Dimensional ( $k_x = 0$ ) Push-over Growth

With  $k_x = 0$ , the wavenumbers are constant so Orr is absent and it is simpler to work with the velocity field directly. The  $\hat{v}$  and  $\hat{w}$  momentum equations together with continuity imply  $\hat{p}_m = 0$  for all  $m$ , leaving the 3 evolution equations

$$\hat{u}_m = -\frac{k_m^2}{Re} \hat{u}_m - \hat{v}_m + \frac{i\beta k_z}{2} (\hat{w}_{m+1} - \hat{w}_{m-1}), \quad (4.1)$$

$$\hat{v}_m = -\frac{k_m^2}{Re} \hat{v}_m, \quad \hat{w}_m = -\frac{k_m^2}{Re} \hat{w}_m, \quad (4.2)$$

where  $k_m^2 = 1 + m^2 k_z^2$ . These indicate that  $\hat{v}_m$  and  $\hat{w}_m$  simply viscously decay in time allowing explicit solutions to be written down as follows

$$\hat{u}_m = e^{-k_m^2 t / Re} \left\{ U_m - V_m t + \frac{i Re \beta}{2 k_z} \left[ \frac{W_{m-1}}{1 - 2m} \left( e^{-(1-2m)k_z^2 t / Re} - 1 \right) - \frac{W_{m+1}}{1 + 2m} \left( e^{-(1+2m)k_z^2 t / Re} - 1 \right) \right] \right\}, \quad (4.3)$$

$$\hat{v}_m = V_m e^{-k_m^2 t / Re}, \quad \hat{w}_m = W_m e^{-k_m^2 t / Re}, \quad (4.4)$$

where  $U_m := \hat{u}_m(0)$ ,  $V_m := \hat{v}_m(0)$  and  $W_m := \hat{w}_m(0)$  are the initial conditions which, by continuity, satisfy  $V_m + m k_z W_m = 0$ . Taking  $Re \rightarrow \infty$  gives the simple  $\hat{u}$  equation

$$\hat{u}_m = U_m - V_m t + \frac{i\beta k_z t}{2} (W_{m+1} - W_{m-1}). \quad (4.5)$$

The push-over effect is produced by the forcing term proportional to the spanwise streak shear,  $\beta k_z$ , and is very similar to the  $-V_m t$  lift-up forcing (normalised to have unit shear) although push-over drives neighbouring spanwise modes while lift-up is direct. Lift-up can be turned off by setting  $V_m = 0$  for  $\forall m$  which, through continuity, forces  $W_m = 0$  for  $m \neq 0$ . Setting  $U_m = 0$  for all  $m$  as well appears an extreme choice for initial conditions but numerical computations indicate that it is close to optimal for  $k_x = 0$  (e.g. at  $\beta = 1$ ,  $T = 5$  and  $Re = 200$ , the error using the extreme choice is only  $\approx 1\%$  of the global optimal gain value). When only  $W_0$  of the initial conditions is non-zero, the gain is

$$\hat{G}^{\text{push}} = e^{-2T/Re} \left[ 1 + \frac{Re^2 \beta^2}{2k_z^2} \left( 1 - e^{-T k_z^2 / Re} \right)^2 \right] \sim 1 + \frac{1}{2} \beta^2 k_z^2 T^2 \quad \text{as } Re \rightarrow \infty. \quad (4.6)$$

assuming  $T \ll Re$  and  $k_z^2 \ll Re/T$  for the asymptotic simplification (we use a  $\hat{\phantom{x}}$  to indicate a quantity not optimised over all initial conditions). This mirrors the result for lift-up: when  $\beta = 0$  is used, choosing only  $(U_1, V_1, W_1) = (0, 1, -1/k_z)$  to be non-zero gives a gain of

$$\hat{G}^{\text{lift-up}} \sim 1 + k_z^2 T^2 / (1 + k_z^2) \quad (4.7)$$

at large  $Re$ . Hence push-over seems to behave very much like lift-up in both the growth possible and the timescales, i.e. growth is ultimately limited by the viscous decay of the spanwise velocities so push-over is ‘slow’.

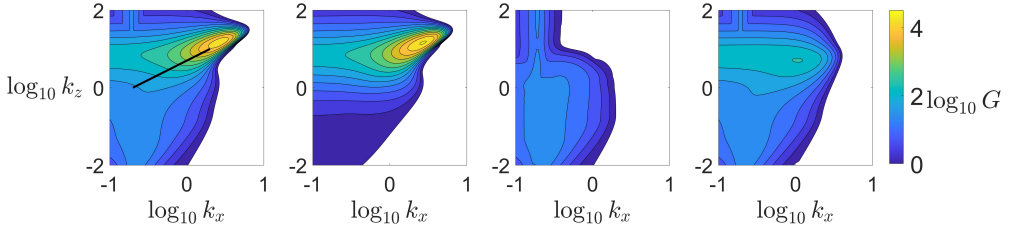


**Figure 5:** Contour plots of the optimal gain over the  $(k_x, k_z)$  wavenumber plane for the parameter set  $\beta = 1$ ,  $T = 5$  and  $Re = 200$ . The truncation value is set to  $M = 20$  and the contour levels are the same across all the plots. Plot (a) shows the full problem (all terms included), while plots (b), (c) and (d) have the lift-up, push-over and Orr mechanisms removed, respectively. The black line traces the wavenumber ranges used for figure 6. The point of this figure is to show that the large growth observed is substantially suppressed when either the push-over or Orr mechanisms are removed, but is largely independent of the lift-up mechanism.

The overall optimal gain in (4.6) can be found by optimising over both  $k_z$  and  $T$ :  $\partial \hat{G}^{push} / \partial k_z = \partial \hat{G}^{push} / \partial T = 0$  requires

$$2k_z^2 T e^{-k_z^2 T / Re} - Re \left( 1 - e^{-k_z^2 T / Re} \right) = 0, \quad (4.8)$$

$$Re^2 \beta^2 \left( 1 - e^{-k_z^2 T / Re} \right) \left[ e^{-k_z^2 T / Re} (1 + k_z^2) - 1 \right] = 2k_z^2. \quad (4.9)$$

The first of these is solved by noticing that the equation reduces to  $2\zeta + 1 - e^\zeta = 0$  with  $\zeta := k_z^2 T / Re$  which has the unique positive solution  $\zeta \approx 1.256$ . Then, using  $e^{-\zeta} = (1 + 2\zeta)^{-1}$  in (4.9) gives the optimal wavenumber as  $\hat{k}_z^{push} = \sqrt{2\zeta}$ , and thus the maximising time and maximal gain for only-non-vanishing- $W_0$  initial conditions as

$$\hat{T}^{push} = \frac{1}{2} Re \quad \text{and} \quad \hat{G}^{push} = \frac{\zeta \beta^2}{e(1 + 2\zeta)^2} Re^2. \quad (4.10)$$

This again shows that the push-over mechanism, in the absence of Orr ( $k_x = 0$ ) and with initial conditions chosen to eliminate lift-up, possesses the same scalings as the lift-up mechanism.

#### 4.2. Transient Growth of Three-Dimensional Perturbations

Larger energy growth occurs for three-dimensional disturbances, where all three mechanisms (lift-up, push-over and Orr) can play a role. Figure 5 displays contours of the optimal gain in wavenumber space for four different scenarios at representative parameter values ( $\beta = 1$ ,  $T = 5$  and  $Re = 200$ ). The left-most plot shows the gain at  $T$  at a given pair of wavenumbers  $(k_x, k_z)$  maximised over all initial conditions for the full equations. The other three plots extending to the right have the three growth mechanisms excluded in turn by artificially removing the terms which drive them: figure 5(b) has lift-up suppressed by removing  $\partial U_B / \partial y$  from the equations; figure 5(c) has push-over suppressed by removing  $\partial U_B / \partial z$ ; and figure 5(d) has the streak advection (the  $\beta \cos(k_z z) \partial \mathbf{u} / \partial x$  term) removed to suppress the ‘spanwise’ Orr mechanism (removing all of the advection changes the whole character of the flow).

A key feature of the figure 5(a) is the global optimal gain indicated by the yellow region, which reaches values of  $\mathcal{G} \approx 10^4$  at  $k_x \approx 2.6$  and  $k_z \approx 14$ . A comparison of this peak and the surrounding region to the same location in the other plots reveals that removing the lift-up mechanism leaves the optimal gain contours almost completely unaltered, while removing either the push-over or spanwise Orr mechanisms reduces the size of gain significantly. This

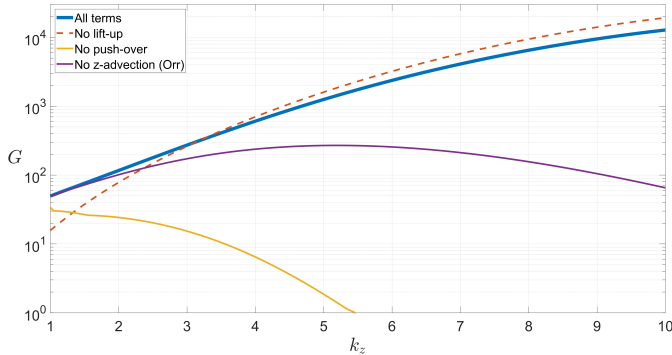


**Figure 6:** A plot showing the optimal gain as  $k_z$  is varied, with  $k_x = k_z/5$  and parameters  $\beta = 1$ ,  $T = 5$  and  $Re = 200$ . The range of  $k_z$  used here is indicated in figure 5(a) using a black line. The blue line represents the gain when all terms are included in the equations (corresponding to the contours in figure 5(a)). The red line shows the gain when the lift-up mechanism is removed, while the yellow line shows gain when the push-over mechanism is removed and the purple line shows gain when the spanwise Orr mechanism is removed (which correspond to the contours in figure 5(b), 5(c) and 5(d), respectively). This plot demonstrates that both the push-over and spanwise Orr mechanisms are crucial for large growth of kinetic energy, even down to some moderate wavenumbers. It also shows that for smaller wavenumbers, a switch occurs and lift-up becomes the dominant growth process.

importance of push-over and lack of importance of lift-up is fully consistent with earlier observations (Lozano-Durán *et al.* 2021; Markeviciute & Kerswell 2024).

The optimal wavenumbers for this global optimal are, however, on the large side for the lower part of the log-layer (see section 2.4) but a line drawn along the major axis of the contours - approximately  $k_z = 5k_x$  - suggests a direction of ‘shallowest’ descent in the wavenumber plane (shown as a black line in figure 5a for  $1 < k_z < 10$ ). Figure 6 shows how the optimal gain behaves along this line for  $1 < k_z < 10$  when the various mechanisms are excluded. At  $k_z = 1$ , removing lift-up is actually more detrimental to the gain than removing either spanwise Orr or push-over, but for  $k_z \gtrsim 3$ , the situation is reversed and mimics that for the global optimal gain. The figure also shows that the presence of lift-up now actually hinders growth (the crossing of blue and red lines at  $k_z \approx 3$ ). This effect is also present in figure 5(b) and is consistent with the observations of Lozano-Durán *et al.* (2021) and figure 7 in Markeviciute & Kerswell (2024).

So, the conclusion is, in this unbounded streaky shear flow at these parameters, wavenumber pairings reaching down to those appropriate for log-layer dynamics show the clear symbiosis of Orr and push-over mechanisms and the unimportance of lift-up as highlighted by the global optimal gain pairing.

#### 4.3. A Simplified Model of the Push-over & Orr Interaction

Remarkably, it is possible to strip the model down to just 2 fields and still retain the symbiotic interaction between push-over and spanwise Orr. There are 3 distinct steps which achieve this. Firstly, the spanwise truncation  $M$  is reduced down to 1 decreasing the number of (complex-valued) fields from  $2(2M + 1)$  (with  $M = 20$  or so) down to 6. Secondly, the symmetry:  $\hat{v}_0 = 0$ ,  $\hat{v}_1 = -\hat{v}_{-1}$  and  $\hat{\eta}_1 = \hat{\eta}_{-1}$  appropriate for the sinuous mode (discussed in

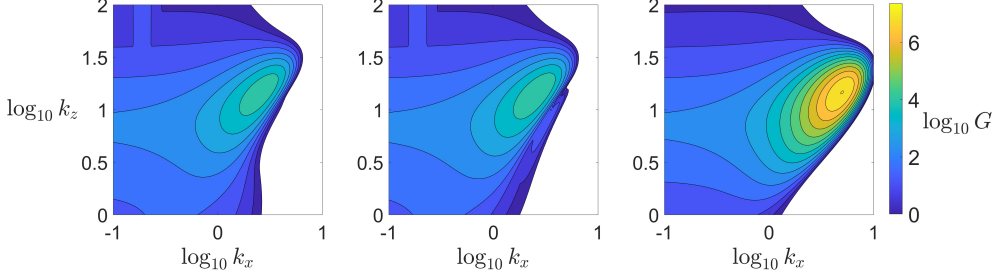


**Figure 7:** A sequence of contour plots showing the optimal gain in wavenumber space, close to the optimal pair, for the parameter set  $\beta = 1$ ,  $T = 5$  and  $Re = 200$ . The colour bar is shown on the right hand side and is the same for all three plots. Plot (a) has truncation value  $M = 20$ , (b) has  $M = 1$  and (c) has  $M = 1$  with the sinuous symmetry used and  $\hat{v}_1$  removed. This figure demonstrates that the underlying growth process is present in all three cases with the reduced model harbouring significantly enhanced growth.

Schoppa & Hussain 2002) is imposed so 6 becomes 3 fields. These evolve as follows

$$\frac{d\hat{v}_1}{dt} = -\frac{k_1^2}{Re}\hat{v}_1 + \frac{2k_x(1-k_x t)}{k_1^2}\hat{v}_1 - \frac{\beta k_z(1-k_x t)}{k_1^2}\hat{\eta}_0, \quad (4.11)$$

$$\frac{d\hat{\eta}_0}{dt} = -\frac{k_0^2}{Re}\hat{\eta}_0 - i\beta k_x \hat{\eta}_1 + \frac{\beta k_x^2 k_z(1-k_x t)}{h_1^2}\hat{v}_1 + \frac{i\beta k_x k_z^2}{h_1^2}\hat{\eta}_1, \quad (4.12)$$

$$\frac{d\hat{\eta}_1}{dt} = -\frac{k_1^2}{Re}\hat{\eta}_1 - \frac{i\beta k_x}{2}\hat{\eta}_0 - ik_z \hat{v}_1 + \frac{i\beta k_z^2}{2k_x}\hat{\eta}_0, \quad (4.13)$$

where, recall,  $k_m^2 := k_x^2 + (1-k_x t)^2 + m^2 k_z^2$ . And finally,  $\hat{v}_1$  can be jettisoned meaning equation (4.11) is ignored and  $\hat{v}_1$  set to zero in the  $\hat{\eta}$  equations. This removes lift-up (the  $-ik_z \hat{v}_1$  term in (4.13)) and an Orr contribution from the third term on the rhs of (4.12). The fact that the term involving  $\hat{v}_1$  in (4.12) is only an Orr term, and further that (4.12) contains no push-over contributions at all, is non-trivial; the details are presented in Appendix A. This leaves simply

$$\frac{d\hat{\eta}_0}{dt} = -\frac{k_0^2}{Re}\hat{\eta}_0 - \overbrace{\frac{i\beta k_x^3}{k_x^2 + k_z^2}\hat{\eta}_1}^{\text{Orr}}, \quad (4.14)$$

$$\frac{d\hat{\eta}_1}{dt} = -\frac{k_1^2}{Re}\hat{\eta}_1 + \frac{1}{2}i\beta k_x \left[ \underbrace{\frac{k_z^2}{k_x^2}}_{\text{Push}} \underbrace{-1}_{\text{Orr}} \right] \hat{\eta}_0, \quad (4.15)$$

where the labels ‘Push’ and ‘Orr’ indicate the source of the remaining terms in the governing equations and the associated physical mechanism (see the discussion in §4.2). Note here that the Orr terms vanish with  $\beta$  so they are ‘spanwise’ Orr terms due to the streak advection. The *a posteriori* justification for such a drastic reduction is provided by figure 7 which shows the gain in the full ( $M = 20$ ) system (the same data as figure 5(a) but replotted over a smaller wavenumber area and with different contour levels), the gain produced by the  $M = 1$  reduction, and the reduced model (4.14)-(4.15). This comparison clearly shows that: i) the  $M = 1$  reduction is surprisingly effective in retaining the gain behaviour and ii) the reduced model also retains the global optimal gain feature and in fact, as also observed, experiences

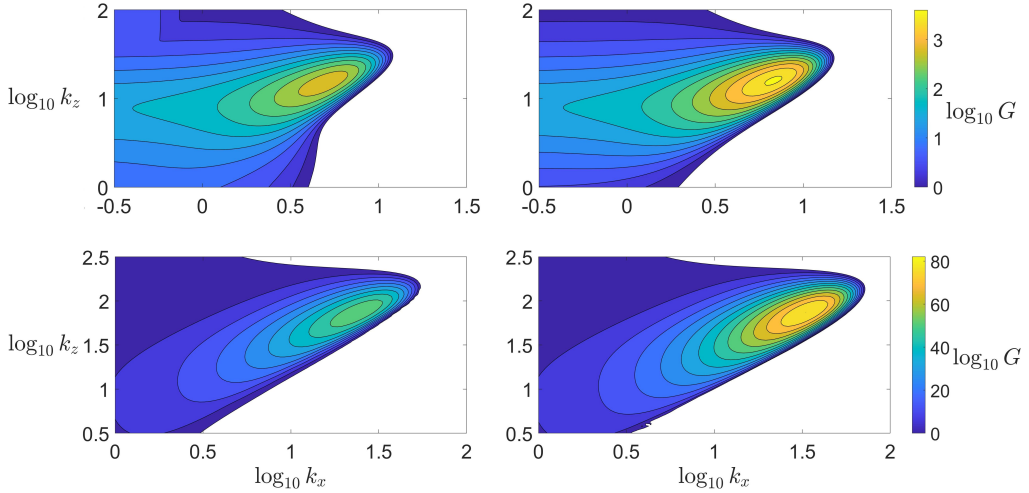


**Figure 8:** Contour plots in wavenumber space of the optimal gain for  $\beta = 1$  (upper) and  $\beta = 5$  (lower), with other parameters set to  $T = 2$ ,  $Re = 100$ . The first column shows the full model with truncation  $M = 20$  while the second column shows the reduced two-variable model given by equations (4.14) and (4.15).

significantly enhanced growth with lift-up removed. Figure 8 shows this picture is repeated for smaller  $Re = 100$  and target time of  $T = 2$  but a larger  $\beta = 5$  value (note the increase in contour scale for  $\beta = 5$  compared with  $\beta = 1$  which is consistent with (4.17)).

For  $Tk_1^2 \ll Re$ , diffusion can be dropped and  $\hat{\eta}_1$  eliminated to produce a particularly simple second order ODE in time for  $\hat{\eta}_0$ :

$$\frac{d^2 \hat{\eta}_0}{dt^2} = \frac{1}{2} \beta^2 k_x^2 \left[ \overbrace{\frac{k_x^2}{k_x^2 + k_z^2}}^{\text{Orr}} \right] \left[ \overbrace{\frac{k_z^2}{k_x^2}}^{\text{Push}} \overbrace{-1}^{\text{Orr}} \right] \hat{\eta}_0 = \frac{1}{2} \beta^2 k_x^2 \left[ \frac{k_z^2 - k_x^2}{k_z^2 + k_x^2} \right] \hat{\eta}_0. \quad (4.16)$$

Providing  $k_z > k_x$ , this has exponential growth *if and only if* both push-over and spanwise Orr are present. This exponential growth (which also requires  $k_x \neq 0$ ) does not signal linear instability because diffusion will ultimately overpower it. For a general  $k_x$ , the time for this cessation of growth is given by the balance  $\beta k_x \sim k_x^2 T^2 / Re$  so  $T = O(\sqrt{\beta Re / k_x})$  and then a prediction for the optimal growth for a *given*  $k_x \lesssim O(Re)$  is

$$G \sim e^{\sqrt{\alpha \beta^3 k_x Re}}, \quad (4.17)$$

where  $\alpha = \frac{1}{2}(k_z^2 - k_x^2)/(k_z^2 + k_x^2)$  is  $O(1)$ . Formally, if  $T \gtrsim O(1)$ , this is maximized for  $k_x = O(Re)$  beyond which diffusion dominates giving a massive gain of  $O(e^{\alpha_1 Re})$  ( $\alpha_1$  being a  $Re$ -independent number). This prediction is confirmed in the 2-variable model *and* for the full system: see Figure 9. This also shows good correspondence between the optimal wavenumbers in each system which all scale linearly with  $Re$ . Figure 9 also confirms that a push-over-less system has no such exponential growth.

However, this overall optimal gain is not the one of practical interest as  $k_z = O(Re)$  (figure 9 actually has  $k_z \sim 0.075Re$  and  $k_x \sim 0.012Re$ ) represents unrealistically large streak shear. If, instead  $k_z = O(1)$  (and hence  $k_x = O(1)$ ), the gain is reduced but still substantial at  $O(e^{\alpha_2 \sqrt{Re}})$  generated over  $O(\sqrt{Re})$  ‘intermediate’ times ( $\alpha_2$  being another constant). This exponential dependence of gain on  $\sqrt{Re}$  is very surprising given that the Orr and push-over

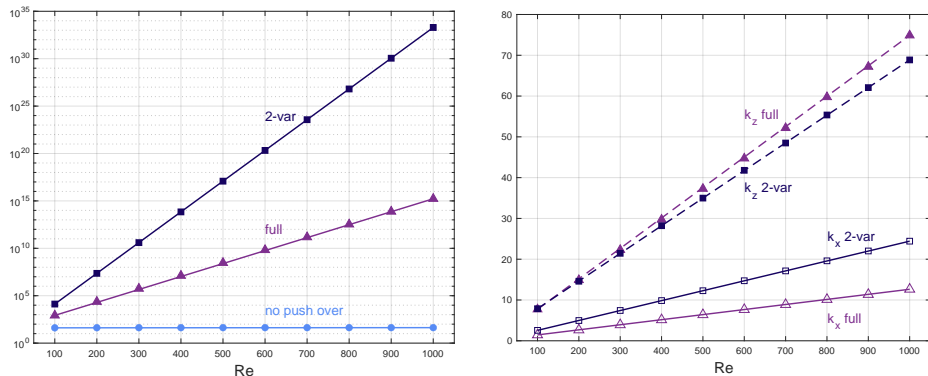


**Figure 9:** Left plot shows the global optimal gain  $\mathcal{G}$  as a function of  $Re$  for  $\beta = 1$ ,  $T = 5$  using the full ( $M = 20$ ) system problem (purple triangles), the reduced 2-variable model (dark blue squares) and the full system with push-over removed (dull blue circles). The lines drawn through the data are the straight lines between the extreme points of each data set indicating that the full system has the same  $\mathcal{G} \sim e^{\alpha Re}$  behaviour as the 2-variable model albeit with a smaller  $\alpha$ . The push-over-less system does not have this exponential dependence. Right plot compares the optimal wavenumbers between the full system and the reduced 2-variable model (the symbols). Lines through the data (drawn as in the Left plot) indicate that all wavenumbers scale linearly with  $Re$ .

mechanisms in isolation only give gains which scale like  $Re^2$  and then only over ‘slow’ times of  $O(Re)$  (e.g. see §3 and §4.1).

Finally, we recall that Figure 7(b) indicates that when  $\hat{v}_1$  is present (or lift-up retained), the gain is reduced by possibly two orders of magnitude but the topography of the gain over the wavenumber plane is unchanged. This is consistent with an earlier observation made from Figure 6 that lift-up can actually hamper the Orr-push-over interaction.

#### 4.4. Mechanism

The detailed mechanism by which the optimal disturbance grows is clearest when examined in primitive variables. Concentrating on the dominant growth mechanism in each of the vorticity equations, (4.14) & (4.15), the closed loop of processes is as follows.

(i) The spanwise velocity perturbation  $\hat{w}_0 := i\hat{\eta}_0/k_x$  ‘pushes over’ (advects) the base streak velocity  $\beta \cos(k_z z) \hat{x}$  to create wavy streaks  $\hat{u}_1$  (and so  $\hat{\eta}_1$ ) via the projection of the term  $\hat{w}_0 \frac{\partial}{\partial z} U_B$  onto the  $\hat{u}_1$  equation.

(ii) These wavy streaks drive a concomitant spanwise field  $\hat{w}_1$  through continuity ( $k_x \neq 0$ ).

(iii) This spanwise field  $\hat{w}_1$  then drives  $\hat{w}_0$  to close the loop by the ‘spanwise’ Orr mechanism i.e. streak advection of  $\hat{w}_1$  given by the projection of the  $\beta \cos(k_z z) ik_x \hat{w}_1$  term onto the  $\hat{w}_0$  equation.

This is for the sinuous mode ( $u/w$  is antisymmetric/symmetric across the streak midplane):  $\hat{w}_0$  vanishes for the varicose mode.

## 5. Discussion

In this paper, motivated by recent numerical experiments on near-wall turbulence by Lozano-Durán *et al.* (2021), we have considered Kelvin’s unbounded, constant-shear model augmented by a spatially-periodic spanwise shear to include streaks. This addition allows a little-studied transient growth mechanism - ‘push-over’ - to be explored along with its interactions with the more familiar Orr and lift-up mechanisms. Consistent with the findings of Lozano-Durán *et al.* (2021) and subsequent analysis by Markeviciute & Kerswell (2024), this model clearly shows that the Orr and push-over mechanisms can combine to produce considerably enhanced transient growth over that produced individually, and that lift-up is unimportant, actually tending to reduce peak growth (although, of course, lift-up is believed central for the roll-to-streak regenerative process). The heart of this symbiotic interaction is laid bare in equation (4.16) of a stripped down version of the model which shows that there is actually exponential growth when both Orr and push-over are present but only oscillatory behaviour otherwise. Due to the sheared (divergent)  $y$ -shearwise wavenumber, diffusion always eventually overpowers this growth (which is therefore only transient and not a linear instability), but during the time before this happens, huge growth scaling like  $e^{\alpha_1 Re}$  can occur over ‘fast’  $T = O(1)$  times. Even restricting the wavenumbers considered to be  $O(1)$  appropriate for a turbulent boundary layer can produce growths scaling like  $e^{\alpha_2 \sqrt{Re}}$  over ‘intermediate’  $T = O(\sqrt{Re})$  times (with  $\alpha_1$  and  $\alpha_2$  constants). This of course is in marked contrast to the algebraic growth factors associated with Orr and lift-up, and now also shown here for push-over in isolation (see (4.10)), of gain  $\sim Re^2$  over ‘slow’  $T = O(Re)$  times.

The advantage of considering such a simple model here should be clear. It has allowed us to extract the relevant  $Re$  scalings of the various transient growth processes active both in terms of energy growth *and* timescale, and thereby identify clearly their relative strengths. The key growing disturbance found here is a ‘sinuous’ mode consistent with the original work of Schoppa & Hussain (2002). What we have done is uncover why the growth they found is large and clarify its dependence on  $Re$ . Even just considering Kelvin’s original model (no streaks) exposes the oversimplification of labelling mechanisms with one timescale based on what turns it off. Orr is considered ‘fast’ and lift-up ‘slow’ yet both give the same levels of growth at  $T = O(1)$  - see (3.4) and (4.7) - and their overall optimal gains are both achieved at  $T = O(Re)$  and scale similarly with  $Re^2$  - see (3.5) and (3.6). Just to complicate matters, the push-over mechanism behaves exactly equivalently - see (4.6) and (4.10) - so there is no timescale puzzle: they all operate across inertial and viscous times. What perhaps *is* a surprise is that the relevant Orr mechanism is based on *spanwise* (streak) advection rather than the usual ‘wall-normal’ advection.

Transient growth is now appreciated to be generic in shear flows and the gain is normally assumed to scale algebraically with  $Re$  such as  $G \sim Re^2$ , for example, seen in plane Couette, channel, pipe and Blasius flows (e.g. see Table 4.1 in Schmid & Henningson 2001). Finding  $G \sim e^{\alpha Re^\gamma}$  here (for some constants  $\alpha$  and  $\gamma$ ) is unusual but not unique. Biau (2016) found  $G \sim e^{\alpha Re}$  for the transient growth in Stokes’s second problem (an oscillating plate bounding a semi-infinite domain of fluid at rest at infinity) and similar gains have been observed in the flow over a backward-facing step (Blackburn *et al.* 2008) and the flow through an expanding pipe (Cantwell *et al.* 2010).

Finally, and more broadly, our work here has shown how Kelvin’s nearly 140 year old model can be usefully extended to unbounded flows which are not just a linear function of space. If the nonlinearity is small/perturbative, one can expect weak coupling between Kelvin modes and then retaining just a pair or triplet of modes (exploiting any symmetries present) may be enough to capture the relevant dynamics as found here. These reduced systems are

then almost as manageable as a single Kelvin mode and can still give great insight due to their accessibility.

**Funding.** W.O. acknowledges financial support from EPSRC in the form of a studentship.

**Declaration of interests.** The authors report no conflict of interest.

**Author ORCIDs.**

William Oxley, <https://orcid.org/0000-0001-7434-0292>;

Rich R. Kerswell, <https://orcid.org/0000-0001-5460-5337>.

## Appendix A. The Absence of Push-Over in the Evolution of $z$ -independent Vorticity

This appendix explains the reason for the absence of any push-over contributions in the evolution equation (4.12) for  $\hat{\eta}_0$ . This is not a trivial fact when using (2.5) as a starting point as an Orr and a push-over term must be combined using continuity to arrive at the term involving  $\partial v/\partial y$ . The source of all the terms can be identified more clearly by starting with the original momentum equation given by (2.2) (where the terms associated with each physical mechanism are clear), and advancing towards equations (2.4) and (2.5) without making any simplifications or cancellations. The final two terms in (2.5) are broken down as

$$\underbrace{-\beta k_z \sin(k_z z) \frac{\partial u}{\partial x}}_{\text{Orr}} - \underbrace{\beta k_z \sin(k_z z) \frac{\partial w}{\partial z}}_{\text{Push}} - \underbrace{\beta w k_z^2 \cos(k_z z)}_{\text{Push}}, \quad (\text{A } 1)$$

where the push-over contributions shown here are, in fact, the only push-over terms present in the evolution equation for  $\eta$  (the advection term in (2.5) is associated with Orr while the  $\partial v/\partial z$  term is associated with lift-up).

To proceed towards equation (4.12), the Kelvin modes in (2.7) are used with  $M = 1$  along with the sinuous symmetry property discussed in section 4.3. The variables can be written in a reduced manner, in particular  $w = [\hat{w}_0 + 2 \cos(k_z z) \hat{w}_1] e^{i[k_x x + (1 - k_x t)y]}$ . The terms labelled as push-over in (A 1) are then simplified to

$$2\beta k_z^2 \sin^2(k_z z) \hat{w}_1 - 2\beta k_z^2 \cos^2(k_z z) \hat{w}_1 - \beta k_z^2 \cos(k_z z) \hat{w}_0, \quad (\text{A } 2)$$

where the exponential multiplication factor is removed for clarity. The first two terms are merged to produce a quantity involving  $\cos(2k_z z)$ , which shows that there are no  $z$ -independent contributions found from the push-over mechanism; it will not contribute in the evolution equation for the  $z$ -independent component of vorticity,  $\hat{\eta}_0$ . This makes it clear that the  $\hat{v}_1$  term in (4.12) (that is subsequently ignored) is only of Orr origin, as is the  $\hat{\eta}_1$  term that is retained.

The last term in (A 2) also produces the full push-over contribution to the  $\hat{\eta}_1$  evolution equation given by (4.13). The identification of Orr and lift-up is then made more simple as any remaining terms will be an Orr contribution if and only if they contain a factor of  $\beta$ .

## REFERENCES

- BAYLY, B. J. 1986 Three-dimensional instability of elliptical flow. *Phys. Rev. Lett.* **57**, 2160–2163.
- BIAU, D. 2016 Transient growth of perturbations in Stokes oscillatory flows. *J. Fluid Mech.* **794**, R4 (10 pages).
- BLACKBURN, H. M., BARKLEY, D. & SHERWIN, S. J. 2008 Convective instability and transient growth in a flow over a backward-facing step. *J. Fluid Mech.* **603**, 271–304.

- BUTLER, KATHRYN M. & FARRELL, BRIAN F. 1993 Optimal perturbations and streak spacing in wall-bounded turbulent shear flow. *Phys. Fluids A* **5** (3), 774–777.
- CANTWELL, C.D., BARKLEY, D. & BLACKBURN, H. M. 2010 Transient growth analysis of flow through a sudden expansion in a circular pipe. *Phys. Fluids* **22**, 034101.
- CASSINELLI, A., DE GIOVANETTI, M. & HWANG, Y. 2017 Streak instability in near-wall turbulence revisited. *J. Turbul.* **18**, 443–464.
- CRAIK, A. & CRIMINALE, W. 1986 Evolution of wavelike disturbances in shear flows: A class of exact solutions of the Navier-Stokes equations. *Proc. Roy. Soc. London A* **406**, 13.
- CRAIK, A. D. D. 1988 A class of exact-solutions in viscous incompressible magnetohydrodynamics. *Proc. Roy. Soc. A* **417**, 235–244.
- CRAIK, A. D. D. 1989 The stability of unbounded 2-dimensional and 3-dimensional flows subject to body forces - some exact solutions. *J. Fluid Mech.* **198**, 275–292.
- ELLINGSEN, T. & PALM, E. 1975 Stability of linear flow. *Phys. Fluids* **18** (4), 487–488.
- FARRELL, B. F. & IOANNOU, P. J. 1993 Optimal excitation of three-dimensional perturbations in viscous constant shear flow. *Phys. Fluids A* **5** (6), 1390–1400.
- HAMILTON, J. M., KIM, J. & WALEFFE, F. 1995 Regeneration mechanisms of near-wall turbulence structures. *J. Fluid Mech.* **287**, 317–348.
- HARTMAN, R. J. 1975 Wave propagation in stratified shear-flow. *J. Fluid Mech.* **71**, 89–104.
- HOEPPFNER, J., BRANDT, L. & HENNINGSON, D. S. 1995 Transient growth on boundary layer streaks. *J. Fluid Mech.* **537**, 91–100.
- JIAO, Y., HWANG, Y. & CHERNYSHENKO, I. S. 2021 Orr mechanism in transition of parallel shear flow. *Phys. Rev. Fluids* **6** (2).
- JIMENEZ, J. 2012 Cascades in wall-bounded turbulence. *Ann. Rev. Fluid Mech.* **44**, 27–45.
- JIMENEZ, J. 2013 How linear is wall-bounded turbulence. *Phys. Fluids* **25**, 110814 (20 pages).
- JIMENEZ, J. 2018 Coherent structures in wall-bounded turbulence. *J. Fluid Mech.* **842**, P1.
- JIMENEZ, J. & PINELLI, A. 1999 The autonomous cycle of near-wall turbulence. *J. Fluid Mech.* **389**, 335–359.
- KELVIN, L. 1887 Stability of fluid motion: rectilinear motion of viscous fluid between two parallel plates. *Phil. Mag.* **24** (5), 188–196.
- KERSWELL, R. R. 1993 The instability of precessing flow. *Geophys. Astrophys. Fluid Dynam.* **72**, 107–144.
- LANDAHL, M. 1980 A note on an algebraic instability of inviscid parallel shear flows. *J. Fluid Mech.* **98**, 243–251.
- LANDMAN, M. J. & SAFFMAN, P. G. 1987 The 3-dimensional instability of strained vortices in a viscous-fluid. *Phys. Fluids.* **30**, 2339–2342.
- LOZANO-DURÁN, A., CONSTANTINO, N. C., NIKOLAIDIS, M.-A. & KARP, M. 2021 Cause-and-effect of linear mechanisms sustaining wall turbulence. *J. Fluid Mech.* **914**, A8.
- MARCUS, P. S. & PRESS, W. H. 1977 On Green's functions for small disturbances of plane Couette flow. *J. Fluid Mech.* **79**, 525–534.
- MARKEVICIUTE, V. K. & KERSWELL, R. R. 2024 Threshold transient growth as a criterion for turbulent mean profiles. *J. Fluid Mech.* **996**, A32.
- MIYAZAKI, T & FUKUMOTO, Y. 1992 3-Dimensional instability of strained vortices in a stable stratified fluid. *Phys. Fluids* **4**, 2515–2522.
- MOFFATT, H. 1967 *The interaction of turbulence with strong shear*. Moscow, June 1965, eds A.M. Yaglom and V. I. Tatarsky (Nauka, Moscow, 1967).
- ORR, W. M. 1907 The stability or instability of the steady motions of a perfect liquid and of a viscous liquid. part ii: A viscous liquid. *Proc. R. Ir. Acad. Sect. A* **27**, 69.
- PANTON, R. L. 2001 Overview of the self-sustaining mechanisms of wall turbulence. *Prog. Aerop. Sci.* **37**, 341–383.
- RICHARDSON, L. F. 1922 *Weather prediction by numerical process*. Cambridge University Press.
- ROBINSON, S. K. 1991 Coherent motions in the turbulent boundary layer. *Ann. Rev. Fluid Mech.* **23**, 601–639.
- SALHI, A. & CAMBON, C. 2010 Stability of rotating stratified shear flow: An analytical study. *Phys. Rev. E.* **81**, 026302.
- SCHMID, P. J. & HENNINGSON, D. S. 2001 *Stability and Transition in Shear Flows*. Springer-Verlag, New York.
- SCHOPPA, W. & HUSSAIN, F. 2002 Coherent structure generation in near-wall turbulence. *J. Fluid Mech.* **453** (1), 57–108.

- SMITS, A. J., MCKEON, B. J. & MARUSIC, I. 2011 High-Reynolds number wall turbulence. *Ann. Rev. Fluid Mech.* **43**, 353–375.
- TUNG, K. K. 1983 Initial-value problems for Rossbywaves in a shear-flow with critical-level. *J. Fluid Mech.* **133**, 443–469.
- WALEFFE, F. 1990 The 3-dimensional instability of strained vortices. *Phys. Fluids*. **2**, 76–80.
- WALEFFE, F. 1997 On the self-sustaining process in shear flows. *Phys. Fluids* **9**, 883–900.